AIAA JOURNAL
Vol. 42, No. 8, August 2004

Luminescent Strain-Sensitive Coatings

J. P. Hubner,* P. G. Ifju,† K. S. Schanze,‡ S. Jiang,§ and Y. Liu§
University of Florida, Gainesville, Florida 32611
and
Wissam El-Ratal¶
Visteon Corporation, Sterling Heights, Michigan 48310

The use of novel luminescent coatings and digital imaging to map the in-plane strain field on structural components under static load is described. The technology, referred to as strain-sensitive skin by Visteon Corporation, employs two different approaches: the first uses a luminescent brittle coating (LBC), and the second uses a luminescent photoelastic coating (LPC). A coating consisting of a binder, generally polymeric in nature, and luminescent dye is applied to the surface of a test part by conventional aerosol techniques. The LBC is excited with incoherent ultraviolet or blue illumination, and the corresponding emission is imaged via a digital camera. The relative change in emission intensity is related to the in-plane volumetric strain response for moderate strain levels. The LPC is excited by the same sources after being conditioned with polarizing and retarding optics to create circularly polarized light. The relative change in emission ellipticity, both in magnitude and phase as measured after passing through an analyzing polarizer, are related to the in-plane shear strain and its corresponding principal direction. These techniques offer quantitative, repeatable, and high spatial resolution measurements. Additionally, they are applicable to complex three-dimensional geometries, cost efficient to implement, and suitable to be integrated in the product design cycle in conjunction with finite element analysis tools. Results from a test conducted on an automobile suspension control arm under static loads are presented and discussed.

Nomenclature

D	=	brittle optical sensitivity
h	=	coating thickness
I	=	intensity
K	=	photoelastic optical sensitivity
r	=	emission anisotropy
α	=	analyzer angle
γ	=	shear strain
Δ	=	relative retardation
ε	=	normal strain
θ	=	principal direction
λ	=	wavelength
ϕ	=	polarization efficiency

Subscripts and Superscripts

av	=	average over a sequence of analyzer angles
c	=	center
em	=	emission
ex	=	excitation
H	=	horizontal
max	=	maximum
ref	=	reference (no load applied)
V	=	vertical
1	=	primary in-plane principal direction
2	=	secondary in-plane principal direction
*	=	effective

Presented as Paper 2003-1437 at the AIAA/ASME/ASCE/AHS Structures, Structural Dynamics, and Materials Conference, Norfolk, VA, 7–10 April 2003; received 12 May 2003; revision received 23 October 2003; accepted for publication 7 November 2003.

*Adjunct Assistant Professor, Department of Mechanical and Aerospace Engineering; jph@mae.ufl.edu. Senior Member AIAA.
†Associate Professor, Department of Mechanical and Aerospace Engineering; pgi@mae.ufl.edu.
‡Professor, Department of Chemistry; kschanze@chem.ufl.edu.
§Postdoctoral Research Assistant, Department of Chemistry.
¶Research and Development Technical Specialist, Chassis Division; welratal@visteon.com.

Introduction

THE measurement of strain on structural components, whether induced by mechanical or assembly loads, is an essential step in the product design cycle. Nondestructive-testing tools are necessary to 1) detect critical design areas and overstressed regions on a component early in the design stage without sacrificing the expensive and limited supply of physical prototypes; 2) validate finite element analysis (FEA) models for quality improvement; and 3) predict the analytical service durability for design optimization and six-sigma robustness studies.

The current industry trend is to link physical testing and analytical methods accurately. This combined design concept enables streamlining of the engineering processes, reduction of the number of prototype builds, and minimization of redundant and expensive physical testing without sacrificing quality. With continual advancements in digital imaging and computing, optical-based techniques offer many viable and cost-effective full-field measurement tools to researchers and engineers. Advantages of such newly developed experimental technologies over the traditional point-measurement techniques, that is, strain gauges, include low intrusiveness, continuous full-field measured data, reduced application time, high spatial resolution, and lower cost per measurement point.

In the field of structural analysis, many optical surface measurement techniques exist,[1–10] including but not limited to interferometric, geometric, Moiré, speckle, image correlation, thermoelastic, brittle coating, and photoelastic coating techniques. Each of these tools has useful applications for specific test conditions. This paper focuses on the application of two new approaches to traditional techniques that use compatible instrumentation and provide complimentary information: luminescent brittle[11] coatings (LBC) and luminescent photoelastic[12,13] coatings (LPC). The techniques provide the full-field sum of principal strain and the maximum shear strain on three-dimensional components, respectively. Both approaches are presented in the context of a test performed on the aluminum control arm component of a midsize sedan-class automobile. In general, for each technique, a component is cleaned, coated, cured,

tested, and analyzed over a period of three to five days. By the use of in situ calibration with strain gauges, a strain dynamic range measurement between $\pm 4000\ \mu\varepsilon$, with 2–3% strain resolution of the full range, is typical. These new testing tools have the advantage of being adaptable to different substrates irrespective of size (ranging from a few centimeters to many meters). Test results are suited for identifying potential design flaws of prototypes as well as validating and modifying FEA models.

Experimental Technique

LBC Technique

Reference 11 describes in detail the principles of operation, instrumentation, and analysis procedures for the LBC technique. The technique uses a luminescent coating in which the emitted intensity is sensitive to the sum of principal strains. The coating consists of a luminophor dissolved into a polymer binder, and the resulting solution is sprayed onto the surface of the test part ($\sim$60–80 μm). An elevated-temperature, low-humidity curing environment induces a randomized microcrack network in the coating. Ultraviolet or blue light sources excite the electronic energy states of the luminophors within the coating. Luminescence (the emitting of photons) is one mechanism to relax the excited states back to the ground state. This occurs at a higher wavelength (lower frequency) than the excitation due to the loss of energy in the deactivation process. An applied strain field on the component alters the microcrack morphology, hence, it changes the relative amount of wave-guided luminescence that is emitted (scattered) from the coating and detected by the imager. Figure 1 is a schematic of the basic instrumentation of the LBC technique.

Equation (1) represents the relative intensity change over a moderate strain range:

$$I/I_{\text{ref}} = 1 + D\varepsilon_c \tag{1}$$

where $\varepsilon_c = \varepsilon_1 + \varepsilon_2$ (the center of the Mohr circle), the terms I, I_{ref}, and ε_c are two-dimensional matrices of the spatial field, and the brittle optical sensitivity D ranges between 0.005 and 0.007%/$\mu\varepsilon$ for the coating described in this paper. Normal air-conditioned environments of 20–25°C and 45–60% relative humidity are ideal for testing conditions. The brittle optical sensitivity is relatively independent of temperature, less than 0.01%/°C, when the reference and load images are acquired at the same temperature. If the temperature drifts between the reference and load image acquisitions, then the relative change in the brittle optical sensitivity increases to 0.5%/°C, inducing a larger error in the measured strain. Because the application of the load is not cyclical, as in thermoelastic techniques that measure changes in surface temperature, and the test environment temperature drift is <1°C during image acquisition, there is negligible temperature-induced error. However, due to the hydrophilic nature of the coating, it is in continuous equilibrium with the moisture in the air; thus, the relative humidity is important during testing. Previous tests show that the optical response plateaus between a relative humidity of 45–60%. At lower or higher humidity levels, the coating dries or swells, respectively, decreasing the optical sensitivity.

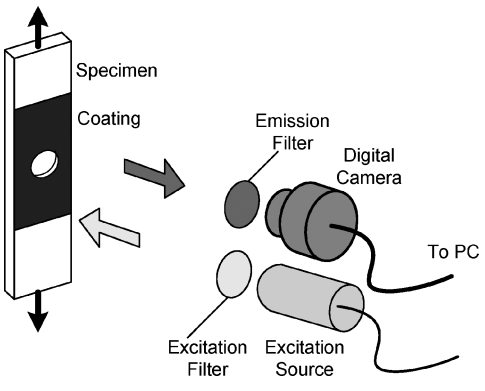

Fig. 1 Schematic of LBC instrumentation.

A digital camera appropriately filtered at the emission wavelength quantifies the emission intensity. Before imaging, initial preloading of the specimen, usually three to five times, will initiate any change in the permanent crack morphology from the postcure state. It is necessary to acquire unloaded (reference) and load images in a darkened environment to eliminate any background light that may excite the coating or pass through the emission filter. Image post-processing procedures include the following: 1) dark-field image correction (subtraction of the camera offset intensity due to readout bias, the thermally generated electronic charge accumulation during the data acquisition, and background light unrelated to the emission of the coating); 2) flat-field image correction (the normalization of the camera pixel-by-pixel gain due to variance in sensitivity and camera lens vignetting); and 3) illumination correction (the normalization of excitation intensity drift between reference and loaded states).

An image registration algorithm aligns (or warps) load images to unloaded images by matching surface target points, determining a six-coefficient second-order polynomial transfer function using a least-square regression, and performing an image-wide bilinear interpolation. The pixel-to-pixel accuracy ranges between 0.1 and 1.0 pixels. Normalizing images with the reference image [I/I_{ref} as shown in Eq. (1)] accounts for variations in spatial illumination and coating thickness. Applying an a priori (with knowledge of specific coating characteristics) or in situ (with corresponding strain gauge data) calibration converts the ratio response to strain. Digital spatial filtering, such as a 3×3 boxcar average, and false-color contouring are useful post-processing tools to decrease spatial noise and highlight strain gradients on the full-field strain maps, respectively.

Because both the LBC technique and thermoelastic techniques are imaging techniques performed in a darkened environment and sensitive to volumetric stresses, it is of interest to briefly comment on the major differences between the two. Thermoelastic techniques require less sample preparation time and no external excitation sources. They are not sensitive to the ambient humidity conditions, but they are sensitive to ambient temperature conditions. Commercial systems are available offering near real-time analysis of components. The cost of scientific-grade infrared digital cameras (12-bit or greater dynamic range) is comparable to that of their visible range counterparts used with LBC. The primary advantage of the LBC technique is that it requires only static loading of the specimen of interest as opposed to dynamic loading, simplifying the test apparatus. Additionally, as described in the next section, the basic instrumentation for the LBC technique is compatible with the LPC technique. The two luminescent techniques in conjunction can be used to determine the maximum principal strain.

LPC Technique

Reference 12 presents the LPC technique in detail, describing a new approach compared to traditional reflective photoelastic coatings and providing a variety of illustrative examples on simple geometries subjected to tensile and torsional loads. The novel LPC technique incorporates a luminescent dye either in an underlayer with a photoelastic overcoat (a dual-layer coating) or directly into the photoelastic coating itself (single-layer coating). The luminescent dye, formulated to retain polarization of the illuminating field, replaces the need for a reflective layer in traditional photoelastic coatings. Benefits derived by the use of luminescence are 1) the separation of excitation from emission via optical filtering, thus eliminating specular reflections and angle-dependent reflection effects; 2) a diffuse emission field on the surface of complex geometries, thus providing the ability to retrieve a much higher and, hence, more spatially uniform, off-axis signal with respect to the imager optical axis; and 3) the potential use of multidirectional excitation and/or detection to decouple the full-field individual principal strains.

Considerable effort was devoted to the improvement of the ease of coating application by development of a spray-on epoxy that does not run when applied to vertical surfaces. The coating is thin (<400 μm), cures overnight, and contains luminescent or absorption additives to account for thickness variation. The thickness of the epoxy can be intentionally varied to 1) target the quarter-fringe

value of the photoelastic overcoat, therefore, eliminating the need for phase-unwrapping and fringe counting as discussed with traditional reflective-based photoelastic coatings[10] and 2) provide the ability to cover a wider dynamic range of strain measurement. Less stringent than the LBC technique, nominal temperature and humidity conditions typical of an air-conditioned testing laboratory are suitable for preparation, application, curing, and testing.

In operation, the strain field on the component due to an applied load transfers to the coating, which in turn changes the stress-induced birefringence of the overcoat. The circularly polarized excitation, of wavelength λ_{ex}, becomes elliptically polarized as it passes through the overcoat. The luminescent undercoat partially retains the polarization state, and then the emission signal of wavelength $\lambda_{em} > \lambda_{ex}$ is further retarded as it passes back through the overcoat. A digital camera, fitted with an analyzer optic (second linear polarizer) and a bandpass interference filter (to reject the excitation signal), measures the corresponding red-shifted emission intensity of the luminescent dye. Figure 2 is a schematic of the basic instrumentation for the LPC technique.

Emission anisotropy r is a ratio of the polarized luminescence component to its total luminescence intensity. Equations (2a) and (2b) (Ref. 14) represent the emission anisotropy:

$$r = \frac{I_{VV} - GI_{VH}}{I_{VV} + 2GI_{VH}} \tag{2a}$$

$$G = \frac{I_{HV}}{I_{HH}} \tag{2b}$$

I_{XY} is the measured emission intensity with the excitation and emission polarizers adjusted to X and Y, respectively. For example, I_{VH} represents the horizontally polarized emission intensity recorded using vertically polarized excitation. An anisotropy of 0.4 is expected for a randomly distributed ensemble of fluorophores that emit polarized light to the same extent as the polarized excitation. Higher values are possible when fluorophores are partially aligned. Figure 3 is a plot of emission anisotropy for a developed luminescent coating

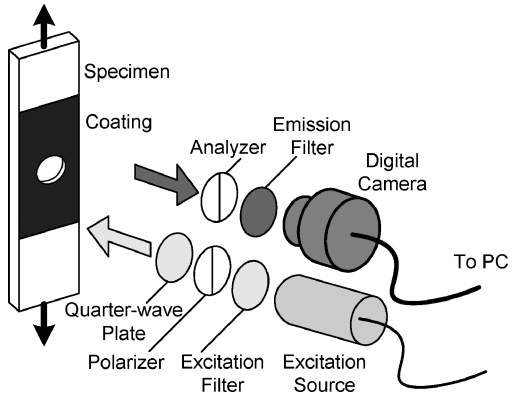

Fig. 2 Schematic of LPC instrumentation.

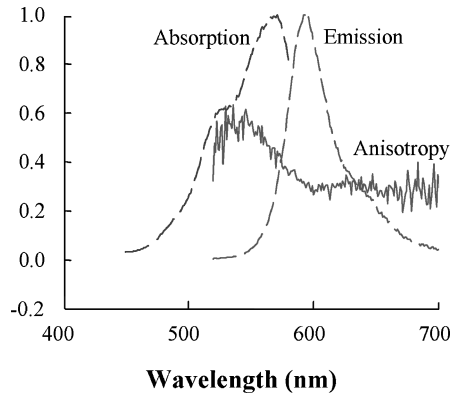

Fig. 3 LPC undercoat: ——, measured anisotropy and – – –, absorption/emission spectra.

with good anisotropy. Values higher than zero (~0.3 as displayed for wavelengths between 500 and 700 nm) indicate the retention of polarization and the viability of the dye.

The in-plane shear strain and its direction are related to the measured subfringe intensity response I, as shown in Eqs. (3a) and (3b) (Ref. 12) when the angle dependence of the excitation and emission transmission through the coating is neglected:

$$I/I_{av} = 1 + \phi \sin(\Delta^*) \sin(2\alpha - 2\theta) \tag{3a}$$

$$\Delta^* = (2\pi K h\gamma/\lambda^*) \tag{3b}$$

where $\gamma = \varepsilon_1 - \varepsilon_2$ (the diameter of the Mohr circle), h is the coating thickness, and $\lambda^* = \lambda_{ex}\lambda_{em}/(\lambda_{ex} + \lambda_{em})$. The optical sensitivity K of the coating described in this paper is approximately 0.12 and is a function of the epoxy birefringence and temperature. Temperature sensitivity is $-2\%/^\circ$C, but thermal curing can decrease this sensitivity to $-0.5\%/^\circ$C. As with the LBC technique, the application of the load is not cyclical, and the test environment temperature drift is $<1^\circ$C during image acquisition, which induces negligible temperature error. The polarization efficiency ϕ is approximately 0.2 and depends on the specific coating formulation and luminescent probe concentration. Preliminary results show that it may be mildly temperature sensitive. Relative humidity effects are not of issue because the working binder is epoxy as opposed to the moisture sensitive binder of the LBC.

At any given load state, the user acquires a series of images at various analyzer angles with the digital camera (generally four angles at 45-deg spacing or eight angles at 22.5-deg spacing). Similar to the LBC technique, it is necessary to acquire the images in a darkened environment (except for the illumination lamps) and to apply dark-field and flat-field corrections. Numerically fitting Eq. 3a, by the use of a nonlinear Levenberg–Marquardt routine, to the sequence of analyzer images at a specific load state results in a pair of maps (two-dimensional matrices) representing the amplitude $\phi \sin \Delta^*$ and phase θ of Eq. (3a). The amplitude, also referred to as the optical strain response (OSR), and phase relate to the magnitude of the maximum shear strain and the principal strain direction, respectively. OSR and phase maps exist for each load level. For a specific applied load, a change in excitation intensity will proportionally increase the image intensity I and the average intensity of the analyzer image sequence I_{av}. Hence, correction for load-to-load excitation drift of the OSR and phase maps is not necessary because the calculations of both are based on the normalized intensity I/I_{av}.

Image registration, described in the preceding section, is necessary to align maps between the load and unloaded (residual) states. For low strains, the relative retardation is much below the quarter-fringe value and $\Delta^* \approx \text{OSR}/\phi$. For higher strains, but still below the quarter-fringe value, $\Delta^* = \sin^{-1}(\text{OSR}/\phi)$. Above the quarter-fringe value, which is dependent on strain, thickness, optical sensitivity, and excitation-emission wavelengths, the OSR is multivalued. As shown in Eqs. (4a–4c), the vector subtraction of the residual relative retardation from the load relative retardation results in the relative retardation due solely from the applied load [Eq. (4b)]:

$$\Delta^* e^{i2\theta} = \Delta_L^* e^{i2\theta_L} - \Delta_R^* e^{i2\theta_R} \tag{4a}$$

$$\Delta^* = \sqrt{\left[\Delta_L^* \sin(2\theta_L) - \Delta_R^* \sin(2\theta_R)\right]^2 + \left[\Delta_L^* \cos(2\theta_L) - \Delta_R^* \cos(2\theta_R)\right]^2} \tag{4b}$$

$$2\theta = \tan 2^{-1}\left[\frac{\Delta_L^* \sin(2\theta_L) - \Delta_R^* \sin(2\theta_R)}{\Delta_L^* \cos(2\theta_L) - \Delta_R^* \cos(2\theta_R)}\right] \tag{4c}$$

where the subscripts L and R represent the load and residual states, respectively.

Finally, due to an inherent weak luminesence of the photoelastic overcoat at wavelengths lower than the luminescent dye, the emission of the coating exhibits wavelength-dependent information. A ratio of the nonpolarized emission intensity at two different wavelengths that use narrowband interference filters shows a linear trend

with thickness. (The calibration by the use of this technique appears to be dependent on the specific test configuration, making it unsuitable as a general technique. Current efforts are toward a more robust thickness correction process.) This dependency is useful for thickness correction of Δ^*. The resulting maps are proportional to strain and can be converted to strain by the use of an a priori or in situ calibration of K/λ^*.

Description of Experiments

An aluminum suspension control arm, shown in Fig. 4 and supplied by Visteon, was the subject of the test. The component was lightly sandblasted, degreased, anodized, and finally coated with the LBC: a melamine formaldehyde resin with rhodamine-B as the luminescent dye ($\sim$80 μm thick). The coating was cured in a temperature–humidity (45°C and 12% relative humidity) controlled environment for 12–15 h to induce a randomized network of microcracks resembling a dry lakebed in appearance. The resulting crack density was on the order of 10–100 per mm. The control arm was tested over a range of static loads from 0 to $\pm$6670 N. Figure 5 is a schematic of the loading fixture. The coating was excited with four blue light-emitting diode (LED) lamps ($\lambda = 465$ nm), two on each side of the control arm at a distance of approximately 2 m. Images from two 16-bit charged-couple device (CCD) cameras, fitted with a standard 50-mm Nikon lens and a 650-nm (40-nm bandpass) interference filter, were acquired at load increments of 1330 N. To improve the signal-to-noise ratio (SNR), an average of 16 images was acquired for each load level by the use of exposure times of 2 s/image or less. A schematic of the LED and CCD position on the right-hand side of the control arm is shown in Fig. 6. The second LED/CCD configuration was positioned on the opposite side of the control arm. After an initial test to identify regions of moderate to high strain response, small patches of the coating were removed on each side of the control arm and instrumented with separator gauges (sensitive to the sum of principal strains) for coating calibration. A subsequent test was performed following the same loading protocol to measure the local strain with the gauges. The measured strains were compared to the ratioed intensity response [Eq. (1)] at the same location to determine a calibration.

On completion of the tests with the LBC, the control arm was cleaned by scraping the coating off of the component after submersion into a bath of acetone diluted with water. The control arm was then degreased and prepared for the undercoat and overcoat application of the LPC. For this test, a fast-curing cellulose acetate coating that incorporated the luminescent dye was sprayed onto the degreased and black-primed surface of the control arm specimen. After a room temperature cure, an epoxy-based photoelastic overcoat that incorporated bis-(4-glycidyloxyphenyl) methane monomer

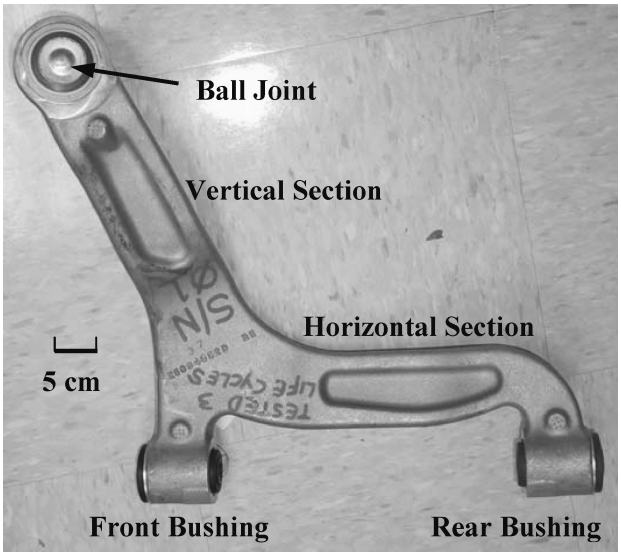

Fig. 4 Aluminum suspension control arm.

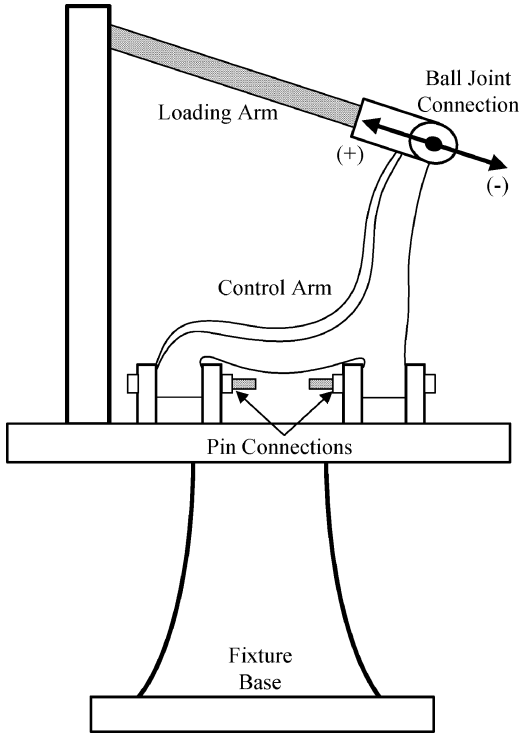

Fig. 5 Schematic of the right-side view of the loading fixture and control arm: maximum load $\pm$6670 N.

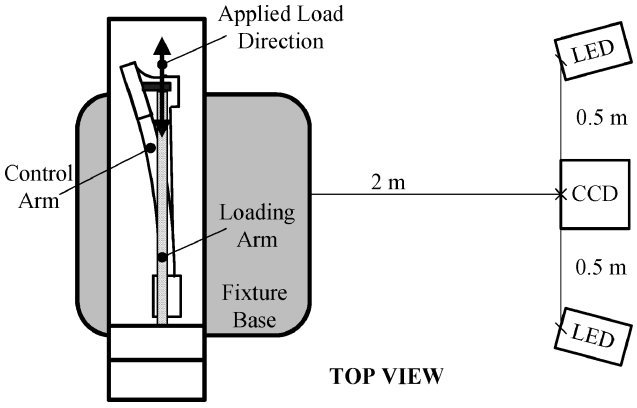

Fig. 6 Top view schematic of CCD camera and LED lamp position (right-side system) relative to the control arm for the LBC test; same equipment alignment (left-side system) was installed on the opposite side of the control arm.

was sprayed on top of the luminescent undercoat in thin multiple layers. The epoxy overcoat was cured by subjection of the specimen to ultraviolet light for a period of 20 min. Overnight thermal curing at elevated temperatures as high as 100°C is also possible and reduces the temperature dependence of the photoelastic optical sensitivity. The nominal thickness was 350 μm, including the undercoat. In general, less part preparation, paint application, and curing time is required for the LPC as compared to that for the LBC.

The same blue LED lamps of LBC technique were used to illuminate the LPC; however, the lamps were coupled with a linear polarizer and a wavelength matched quarter-wave plate to produce circular polarized light. Only one lamp was placed on each side of the control arm at a distance of approximately 2 m. A schematic of the LED and CCD position on the right-hand side of the control arm is shown in Fig. 7. The second LED/CCD configuration was positioned on the opposite side of the control arm. Because of the lower raw intensity response of the LPC (additional optics compared to the LBC), exposure times were increased to as long as 120 s/image. Subsequent enhancements to the formulation have decreased typical exposure times, ranging from 2 to 30 s/image depending on

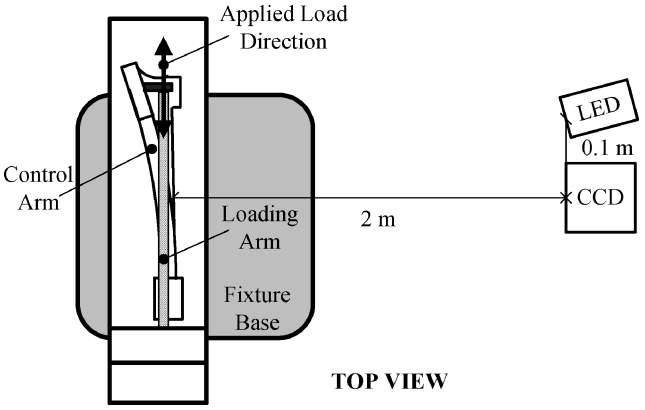

Fig. 7 Top view schematic of CCD camera and LED lamp position (right-side system) relative to the control arm for the LPC test; same equipment alignment (left-side system) was installed on the opposite side of the control arm.

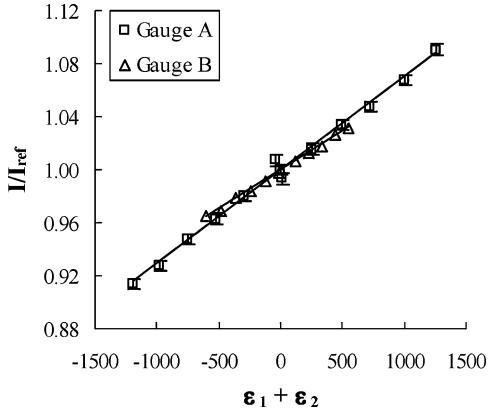

Fig. 8 Calibration of LBC intensity ratio response to the summation of principal strains at two gauge locations (data fitted with a linear regression); corresponding slopes are 7×10^{-5} at gauge A and 6×10^{-5} at gauge B.

the specific test configuration. A 600-nm (40-nm bandpass) interference filter was used to detect the emission. Images were acquired at analyzer angles of 0, 45, 90, and 135 deg. The uncalibrated OSR was used to identify regions of strong response for the placement of two rosette gauges for coating calibration. The loading sequence was repeated to measure the gauge strains and calibrate the OSR.

Results and Discussion

LBC Control Arm Measurements

Raw images were processed as outlined in the preceding sections, and intensity ratio values (I/I_{ref}) were plotted vs the separator gauge measurements ($\varepsilon_1 + \varepsilon_2$) to determine an in situ calibration. Results from gauge A (right side) and gauge B (left side) are shown in Fig. 8. A linear trend is apparent for each gauge. The error bars shown for gauge A (4% of the relative change $I/I_{\text{ref}} - 1$) indicate a 95% confidence interval based on the pixel-to-pixel variation within the interrogated region.

Figures 9a–9c show processed strain maps for both CCD views at the load conditions of +1330, +4000, and +6670 N, respectively. The red color scale indicates a tensile volumetric strain, whereas the blue color indicates a compressive volumetric strain. The pixel density is 10/cm. The control arm was held fixed at the front and rear bushings, and a positive load as defined in Fig. 5 was applied at the ball joint of the vertical section. Key features for this loading configuration are high tensile volumetric strain on the right side of the vertical section approaching $+2000\ \mu\varepsilon$ and high compressive volumetric strain along the arc approaching $-2000\ \mu\varepsilon$.

For repeatability purposes, the loading test was duplicated on the following day. Results were compared over four arbitrary sample regions between the two tests. The measured difference was ±6%

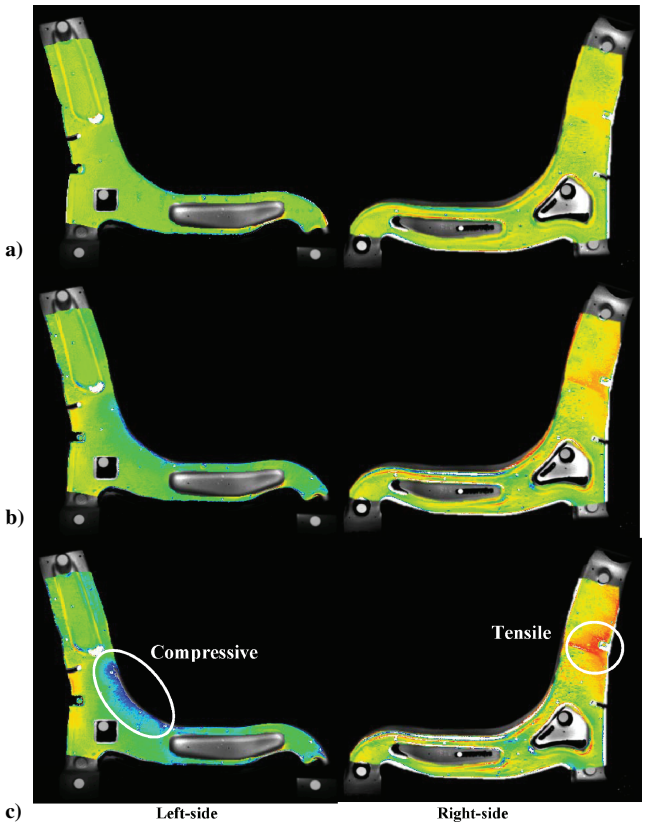

Fig. 9 Strain fields for the a) +1330-, b) +4000-, and c) +6670-N loading conditions as viewed from the two CCD cameras; color scale ranges from −2000 to +2000 $\mu\varepsilon$ (blue–green–red).

of the local strain measurement. In general, a test object coated with LBC can be tested again as long as the coating is not damaged during the test. Over a period of weeks, the coating will still be responsive as long as the environmental conditions are condusive to testing (temperature from 20 to 30°C and relative humidity from 45 to 60%). However, a new calibration would be necessary to compensate long-term age-dependent properties when the same optical set-up is used.

Quantitative full-field volumetric experimental strain results were used by Visteon to validate and modify the analytical FEA model of the control arm. Often, improper assumptions of FEA boundary conditions or constraints result in solutions that neither capture the actual failure locations nor predict the proper levels of strain values. The FEA boundary conditions of the suspension control arm were modified by employment of an iterative optimization process. For accurate results, the FEA model calibration process required the large number of well-distributed discrete experimental strain values provided by the testing technology.

LPC Control Arm Measurements

The control arm with LPC was constrained in the same fashion as the LBC test. As discussed earlier, a sequence of analyzer images were acquired for each load application. The OSR was plotted vs the in-plane shear strain ($\gamma = \varepsilon_1 - \varepsilon_2$) measured from two rosette gauges, one on each side of the control arm, to determine an in situ calibration. Figure 10 is a plot of the calibration results. A near linear trend is visible for the range shown, which indicates that the coating thickness is well below the quarter-fringe value. Error bars (1–2%) indicate a 95% confidence interval based on the pixel-to-pixel variation within the sampled region of interest. Accurate evaluation of coating properties, specifically K and ϕ, before testing could lead to the elimination of strain gauges for calibration purposes.

The coating thickness at various points was measured with an eddy-current coating thickness gauge. The measurements were compared to the ratio of 650- to 600-nm nonpolarized emission intensity

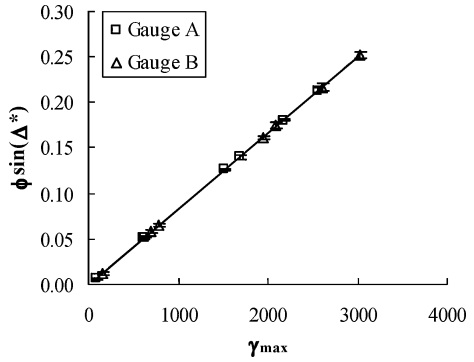

Fig. 10 Calibration of LPC response (subquarter fringe) to the maximum in-plane shear strain at two gauge locations (data fitted with a linear regression); corresponding slope is 8.3×10^{-5} for both gauges.

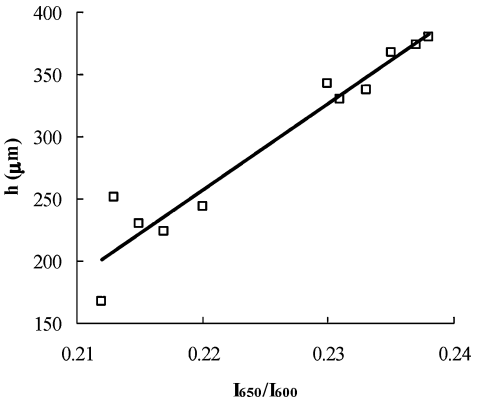

Fig. 11 Thickness calibration curve for LPC.

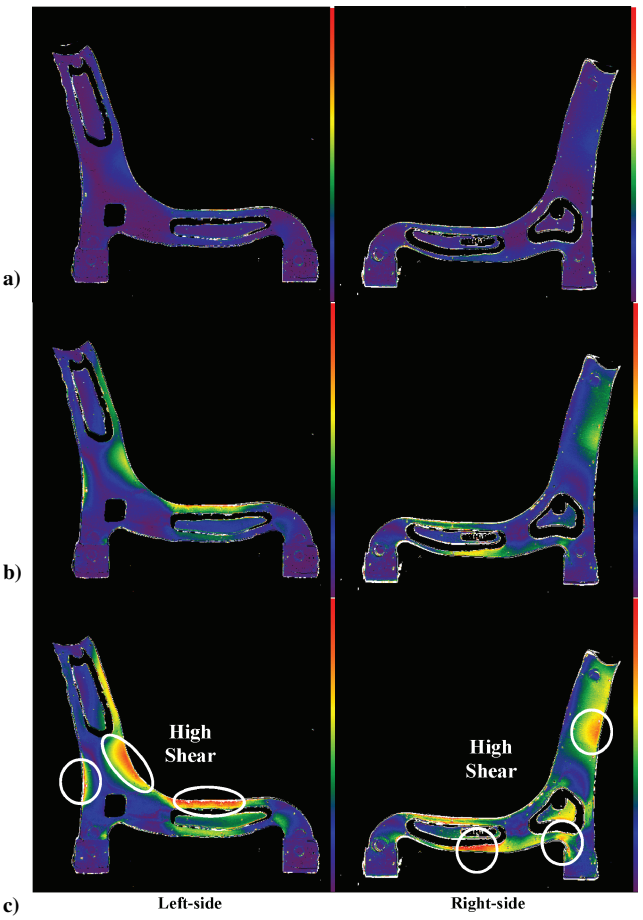

Fig. 12 Shear strain fields for the a) +1330-, b) +4000-, and c) +6670-N loading conditions as viewed from the two CCD cameras; color scale ranges from 0 to +3200 $\mu\varepsilon$ (blue–green–red).

at the same points. The images were collected with 10-nm bandpass interference filters. The thickness calibration results are shown in Fig. 11. Figures 12a–12c show thickness corrected in-plane shear strain results for both CCD views at the load conditions of +1330, +4000, and +6670 N, respectively. The relative pixel density is 10/cm. Regions of high shear strain, approaching 3200 $\mu\varepsilon$ in some areas, are visible along the arc of the control arm (left side) and midway up the vertical section and underneath the horizontal section (right side) as indicated by the red color scale. The LPC results exhibited lower spatial noise as compared to LBC results (2–4%, respectively) due to the continuous nature of the LPC and the discrete microcracked structure of the LBC.

Repeatibility of measurements between successive days was ±4% of the local strain measurement. A test object, coated with LPC, can be tested again as long as the coating is not damaged during the test and the specimen is not under continous load. This makes the LPC technique a possible candidate for monitoring the strain field variation of components in service. Although epoxies are inherently viscoelastic, creeping of the coating is negligible when applied to substrates under short static loads (on the order of minutes). Tensile tests on a continuously loaded specimen show no discernible change

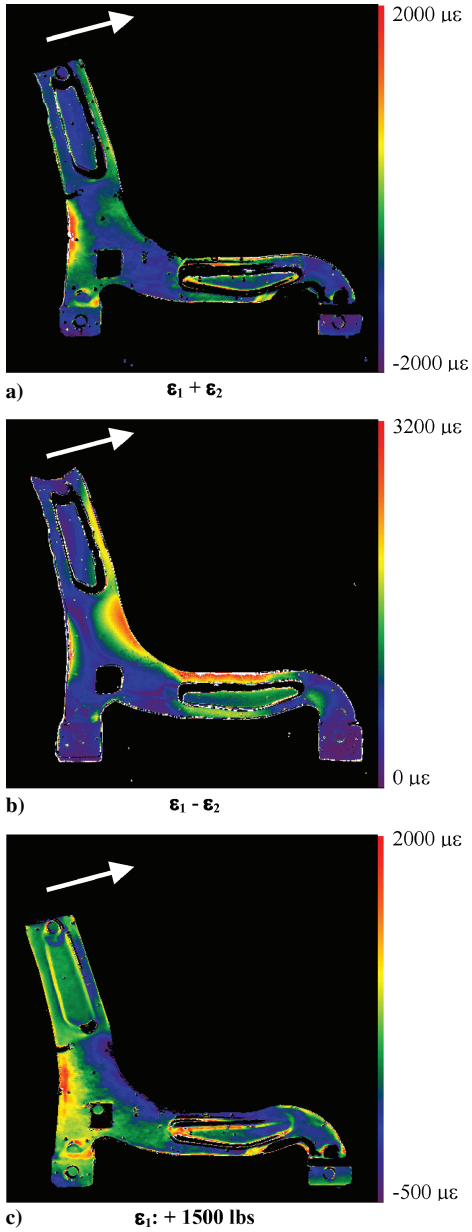

Fig. 13 Determination of the maximum principal strain from the LBC and LPC processed strain maps.

in the OSR outside the noise bands after 1 h and a 4% decrease after 18 h. Because the substrate bears the load, short-term creeping in the coating is negligible. Tensile specimens fabricated out of the epoxy only (not a coating on a metallic substrate) do exhibit more significant rate- and time-dependent mechanical properties.

By the use of results from both LBC and LPC techniques, the individual principal strain magnitudes, ε_1 and ε_2, were determined when the two-equation–two-unknown system was solved, as shown in Eq. (5):

$$\varepsilon_1 + \varepsilon_2 = \varepsilon_c : \varepsilon_1 - \varepsilon_2 = \gamma \tag{5}$$

Results of such analysis are shown in Fig. 13 for the load case of +6670 N. Highest tensile maximum principal strain values (Fig. 13c) are observed to be on the left-side of the vertical section near the front bushing. Along the arc between the vertical and horizontal section is a large region of compressive strain.

Conclusions

Two luminescent coating techniques for measuring in-plane strain have been developed and tested on an automotive component. The first uses a luminescent brittle coating and is sensitive to the sum of principal strains ($\varepsilon_1 + \varepsilon_2$). The second uses a luminescent photoelastic coating that is sensitive to the in-plane shear strain ($\varepsilon_1 - \varepsilon_2$) and principal direction. Both coatings are applied with conventional aerosol techniques. To date, they have been applied to ferrous, nonferrous, and graphite/epoxy specimens, regardless of size, and should be suitable to any substrate in which good adhesion can be achieved. The two coatings require similar excitation and imaging equipment and provide full-field strain results. Physical tests, conducted with these coating techniques, are straightforward and quickly performed within a few days. Strain resolutions of 2–3% of the full dynamic strain range can be achieved. In conjunction with each other, the individual principal strain magnitudes ε_1 and ε_2 can be decoupled. Of the two coatings, the LPC is more environmentally robust, durable, easier to apply, cheaper to implement, and has a higher spatial resolution than the LBC. Additionally, it is suitable for test objects that undergo large displacements/deformations and provides the additional principal strain direction information. Test results have been used by the Visteon Corporation to detect possible failure mode locations of the suspension control arm early in the design stage, without permanently damaging the physical prototype. In addition, the full-field strain data were used to establish proper FEA model boundary conditions, thus improving model quality.

Acknowledgments

The authors thank Visteon Corporation, Chassis Systems, for their sponsorship of this research. Special thanks go to Joseph Rozman and Raymond Milko of Visteon, who assisted with the tests.

References

[1]Daily, J. W., and Riley, W. F., *Experimental Stress Analysis*, 3rd ed., McGraw–Hill, New York, 1991, Chaps. 11 and 15.

[2]Cloud, G. L., *Optical Methods of Engineering Analysis*, Cambridge Univ. Press, New York, 1998.

[3]Rastogi, P. K. (ed), *Topics in Applied Physics: Photomechanics*, Vol. 77, Springer, Berlin, 1999, Chaps. 4–6 and 10.

[4]Post, D., Han, B., and Ifju, P. G., *High Sensitivity Moiré: Experimental Analysis for Mechanics and Materials*, Springer-Verlag, New York, 1994, Chaps. 3–5.

[5]Morse, S., Durelli, A. J., and Sciammarella, C. A., "Geometry of Moiré Fringes in Strain Analysis," *Journal of Engineering Mechanics Division, ASCE*, Vol. 86, 1960, pp. 105–126.

[6]Jones, R., and Wykes, C., *Holographic and Speckle Interferometry*, Cambridge Univ. Press, Cambridge, England, U.K., 1983, Chaps. 2, 3, and 7.

[7]Sutton, M. A., Cheng, M., Peters, W. H., Chao, Y. J., and McNeill, S. R., "Applications of an Optimized Digital Correlation Method for Planar Deformation Analysis," *Image and Vision Computing*, Vol. 4, 1986, pp. 143–150.

[8]Durelli, A. J., Hall, J., and Stern, F., "Brittle Coating," *Handbook on Experimental Mechanics*, edited by A. S. Kobayashi, Prentice–Hall, Englewood Cliffs, NJ, 1987, pp. 516–554.

[9]Zandman, F., Redner, S., and Dally, J. W., *Photoelastic Coatings*, Iowa Press, Ames, IA, 1977, Chap. 6.

[10]Lesniak, J. R., and Zickel, M. J., "Applications of Automated Grey-Field Polariscope," *Proceedings of the SEM Spring Conference on Experimental and Applied Mechanics*, Society of Experimental Mechanics, Bethel, CT, 1998, pp. 298–301.

[11]Hubner, J. P., Ifju, P. G., Schanze, K. S., Jenkins, D. A., Carroll, B. F., Wang, Y., He, P., Brennan, A., and El-Ratal, W., "Full-Field Strain Measurement Using a Luminescent Coating," *Experimental Mechanics*, Vol. 43, No. 1, 2003, pp. 61–68.

[12]Hubner, J. P., Ifju, P. G., Schanze, K. S., Liu, Y., Chen, L., and El-Ratal, W., "Luminescent Photoelastic Coatings," Society of Experimental Mechanics, Paper 263, June 2003.

[13]Hubner, J. P., Ifju, P. G., Schanze, K. S., Jaing, S., Liu, Y., Jenkins, D. A., and El-Ratal, W., *Method and Apparatus for Measuring Strain Using a Luminescent Photoelastic Coatings*, U.S. Patent Application 10/407,602, 4 April 2003.

[14]Lakowicz, J. R., *Principles of Fluorescence Spectroscopy*, 2nd ed., Kluwer Academic/Plenum, New York, 1999, pp. 291–303.

B. Sankar
Associate Editor

Color reproductions courtesy of Visteon Corporation, Chassis Division.